A study of critical factors for the development of aqueous−route based aluminium oxide dielectric

수성 경로 기반 산화물 유전체 개발에 미치는
중요 요소에 관한 연구

2018 년 8월

서울대학교 대학원

융합과학부 나노융합전공

허 재 은

A study of critical factors for the development of aqueous-route based aluminium oxide dielectric

수성 경로 기반 산화물 유전체 개발에 미치는
중요 요소에 관한 연구

2018 년 8월

서울대학교 대학원

융합과학부 나노융합전공

허 재 은

A study of critical factors for the development of aqueous－route based aluminium oxide dielectric

지도교수 김연상

이 논문을 공학석사학위논문으로 제출함

2018 년 8월

서울대학교 대학원

융합과학부 나노융합전공

허 재 은

허재은의 석사학위논문을 인준함

2018 년 5월

위 원 장 ___박 원 철___ (인)

부 위 원 장 ___김 연 상___ (인)

위 원 ___유 지 영___ (인)

A study of critical factors for the development of aqueous-route based aluminium oxide dielectric

Jae-Eun Huh

Program in Nano Science and Technology

Department of Transdisciplinary Studies

The Graduate School of

Seoul National University

Aqueous route method based on a metal aquo complex has attracted a lot of attention because it enables the solution-processed metal oxide thin film with high electrical properties to be prepared in low temperature fabrication condition. However, most studies have

mainly focused on the development of metal oxide semiconductor thin film. For expansive application of the aqueous route based metal oxide films to various flexible fundamental devices, the systematic study for the development of metal oxide insulator film based on the aqueous route method is urgently required.

Here, I propose critical factors for developing high−quality metal oxide insulator thin films based on the aqueous route method. I found that the critical factors including precursor solution temperature and humidity during the spin−coating process strongly affect chemical, physical, and electrical properties of AlO_x insulator thin films. Through the optimization of critical factors, an AlO_x insulator thin film with a leakage current value approximately 10^5 times smaller and a breakdown voltage value approximately $2 \sim 3$ times greater than un− optimized AlO_x was realized. Finally, by introducing the optimized AlO_x insulator thin film to solution−processed InO_x TFTs, I successfully achieved InO_x/AlO_x TFTs with remarkably high average field−effect mobility of ~52 $cm^2V^{-1}s^{-1}$ and on/off current ratio of 10^6 at fabrication temperature of 250 ℃.

....

Table of Contents

List of Figures

List of Tables

Chapter 1. Introduction

1.1 Current Trend in Metal Oxide Dielectrics

In the past decades, metal oxides such as InO_x, ZnO_x, AlO_x, and ZrO_x have received a lot of attention as fundamental materials in future electronics like transparent smart windows, flexible electrochromic windows, flexible energy generating devices, and multifunctional sensors due to their electrical performance and unique properties like flexibility and transparency.[1-5] Accordingly, many efforts have been made to develop the deposition methods to attain high-quality metal oxide thin films.[6,7] Among them, a solution process received attention due to the many advantages as a large-scale and low-cost advanced fabrication process.[3,6,7] However, solution-processed metal oxide thin films typically have lots of defects and traps, which result in relatively poor electrical performance compared to that of vacuum-processed metal oxide thin films.[5] In addition, when the metal oxide thin film is fabricated in low-temperature fabrication conditions for application in flexible electronic devices, various impurities such as carbon-based substances from the precursor solution were not removed in low-temperature annealing process.[8-13] These organic impurities have caused serious problems by lowering film quality and deteriorating

electrical performance, which hinders the practical application of a solution process to fabricate oxide thin films.

1.2 Introduction to Aqueous Route

Recently, an aqueous route method based on a metal aquo complex for solution-processed deposition of metal oxide thin films has been proposed.[14] This method has attracted considerable attention because it enables the solution-processed metal oxide thin film with high electrical properties to be prepared in low temperature (< 300 °C) fabrication conditions. Thus, many researchers have systemically studied the method and identified the critical factors for optimizing solution-processed oxide films based on the aqueous route method.[15-18] Unfortunately, most studies related to the aqueous route method have mainly focused on the metal oxide semiconductor thin film fabrication.[14,19,20] In various fundamental devices such as thin-film transistors (TFT), energy harvesting electronics and memory devices, insulator films are essential. For expansive application of the solution-processed metal oxide films to various flexible fundamental devices, the development of the low-temperature solution-processed metal oxide insulator films is urgently required. For this reason, based on the potentiality of the aqueous route method, researchers have recently attempted to develop a metal oxide insulator thin film based on the aqueous route method.[21-25] However, the systematic study for metal oxide insulator film based on the aqueous route method has not yet been studied.

Accordingly, the critical factors for optimizing the metal oxide insulator thin film based on the aqueous route method have not been identified.

1.3 Two Critical Factors for Developing High-Quality Oxide Dielectrics

Here, I propose critical factors for developing high-quality metal oxide insulator thin films based on the aqueous route method. Depending on the temperature of the precursor solution and the humidity condition during the spin-coating process, dramatic changes in chemical and physical properties of AlO_x insulator thin films that strongly affect the electrical properties were found. An AlO_x insulator thin film with a leakage current value approximately 10^5 times smaller and a breakdown voltage value approximately 2~3 times greater than unoptimized AlO_x was realized by optimizing critical factors. Finally, by introducing the optimized AlO_x insulator thin film to solution-processed InO_x TFTs, I successfully achieved InO_x/AlO_x TFTs with remarkably high average field-effect mobility of ~52 $cm^2V^{-1}s^{-1}$ and on/off current ratio of 10^6 at fabrication temperature of 250 ℃.

Chapter 2. Experimental Process

2.1 Preparation of Precursor Solution

AlO$_x$ precursor solutions (0.2 M) were prepared by dissolving aluminum nitrate hydrate in deionized water, and then solutions were stirred at 500 rpm for 3 days in 25, 30, and 35 °C, respectively. In the case of the InO$_x$ precursor solution (0.2 M), indium nitrate hydrate was dissolved in deionized water. The thermogravimatric analysis (TGA (TGA/DSC 1 STARe system, Mettler Toledo)) was performed under dry air atmosphere with a heating rate of 10 °C min^{-1}. The liquid chromatography－mass spectrometry (LC－MS (LC－Q－TOF, Agilent Technologies)) was performed by injecting 25, 30 and 35 °C precursor solutions in positive ionization mode with each temperature.

2.2 Film Fabrication and Characterization

For the AlO_x films, the AlO_x precursor solutions were filtered through a 0.22 mm syringe filter PTFE(DISMIC 13HP020AN, Advantec, Japan), and spin-coated at a humidity of 10 ~ 50% at 2000 rpm for 30 seconds. Deposited films were soft-baked at 250 ℃ for 1 minute, and they were annealed in a tube-furnace under <10% humidity at 250 ℃ for 4 hours. In the case of the InO_x film, after the AlO_x film was treated by UV-ozone (UVO), InO_x precursor solution was spin-coated under humidity of ~ 10% at 5000 rpm for 30 seconds. And then, the films are soft-baked at 250 ℃ for 1 minute, and were annealed in a tube-furnace under <10% humidity at 250 ℃ for 4 hours. Here, the humidity means the relative humidity at 25 ℃. The morphology images of AlOx films were obtained by optical microscopy (OM) (BX41TF, Olympus) and field emission scanning electron microscope (FESEM) (S-4800, Hitachi). The roughness and thickness of AlOx films investigation of the AlOx films were performed using atomic force microscopy (AFM) (XE100, PSIA).

2.3 Fabrication of the MIM and TFT Devices

For the MIM devices (**Figure 1**), p^{++} silicon wafer as a bottom gate electrode and an aluminum source/drain electrode was deposited on the AlO_x dielectric films. First, the Si substrate was washed with detergent, DI water, acetone and isopropanol by using ultrasonication. After drying with N_2 blowing, Si substrate went through UVO treatment for 20 min. For the TFT (**Figure 2**), the aluminum source and drain electrodes were deposited on the InO_x layer by thermal evaporation with the shadow mask, thickness of 100 nm, width of 1000 μm, length of 50 μm.

Figure 1. Schematic structure of MIM devices.

Al electrode : 100 nm

Channel width : 1000 μm

Channel length : 50 μm

InO_x 10 nm

AlO_x 10 ~ 15 nm
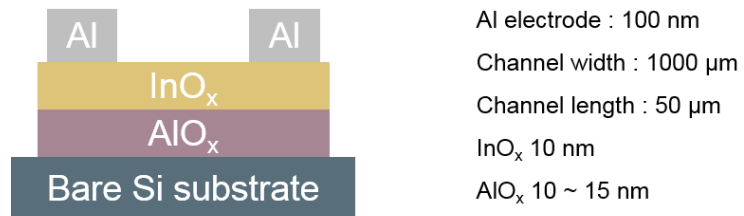
Figure 2. Schematic structure of TFT devices.

2.4 Measurement of the Capacitance and TFT Characterization

The 20 Hz to 1 kHz capacitance of AlO_x were obtained by Agilent 4284A and the 0.5 Hz to 20 Hz capacitance of AlO_x were obtained by BioLogic SP150. The transfer and output characteristics of InO_x/AlO_x TFT were measured by Agilent 4155B semiconductor parameter analyser under dark condition. The field−effect mobility of InO_x/AlO_x TFTs was evaluated by the linear formula.

$$I_D = \frac{W}{L} C_i \mu (V_G - V_T) V_D$$

Chapter 3. Result and Discussion

3.1 Experimental Design to Study Critical Factors for Developing Aqueous Route based Oxide Dielectric

In various metal oxide insulators, AlO_x was chosen due to its high electrical properties as well as high stability as an aqueous solution.[22] In addition, the thermal decomposition temperature for removing impurities in an aluminum aquo complex was small enough to apply it to the low temperature solution process (**Figure 3**). To study the critical factors for developing metal oxide insulator film based on the aqueous route method, I focused on the factors that strongly affect the film properties and easily change in solution－based fabrication processes. Considering the results in previous studies related with the aqueous－route based metal oxide semiconductor films, the temperature of the precursor solution, and the humidity condition during its spin－coating process could be considered suitable factors.[15-18]

In order to find suitable conditions for the atmospheric solution process, the experiment was conducted under temperature and humidity conditions that are controlled in actual atmospheric conditions. Accordingly, the aqueous－route based AlO_x films were

fabricated by a precursor solution with specific temperatures (25, 30, and 35 ℃), and under specific humidity conditions during the spin-coating process (10, 20, 30, 40, and 50%). Here, the precursor solution prepared by different temperatures was maintained at the fixed temperature throughout the period from solution synthesis process to coating process.
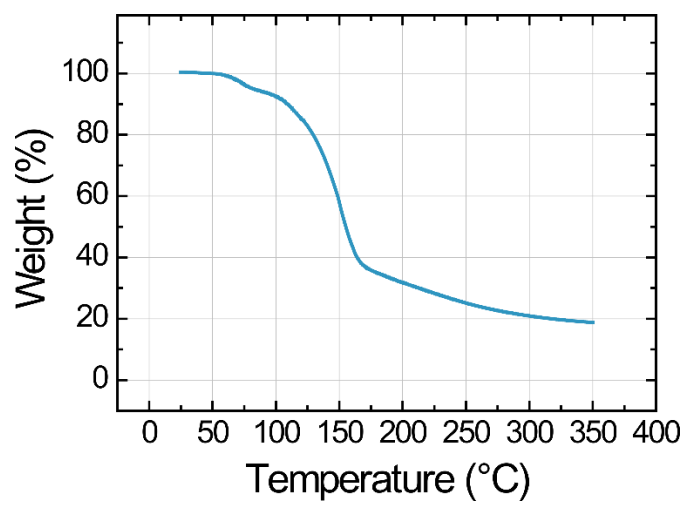
Figure 3. Thermal behavior of the AlO_x precursor xerogel through TGA.

3.2 Analysis of Changes in Electrical Properties of AlO_x Insulator Depending on Two Critical Factors: Temperature of Solution and Humidity Condition during Spin-coating Process

Figure 4 shows J-E characteristics of AlO_x films fabricated, by a precursor solution at different temperatures and under various humidity conditions during the spin-coating process. **Table 1** and **Table 2** show numerical values of breakdown voltage and the current density at 3 $MVcm^{-1}$ in AlO_x films fabricated under the aforementioned conditions. To measure the J-E characteristics of the AlO_x films, a metal-insulator-metal (MIM) structure was used. The "breakdown voltage" is defined as the electric field strength at which the leakage current density reaches 100 μAcm_{-2}. Additionally, to verify the thickness of the AlO_x film, an atomic force microscopy (AFM) analysis was used (**Figure 5**). The height gap is obtained by photolithography and etching process. Film thicknesses of 10, 20, 30, 40, and 50% AlO_x by measuring the height-gap are 11.3, 13.9, 13.5, 13.8, and 13.2 nm, respectively. The AlO_x film fabricated at 10, 20, 30, 40, and 50% relative humidity during the spin-coating process is denoted as 10, 20, 30, 40, and 50% AlO_x, respectively. According to **Figure 4**, depending on the changes in humidity during the spin-

coating process and temperature of precursor solution, the breakdown voltage and leakage current of AlO_x are considerably changed.

In terms of the change of the breakdown voltage of the AlO_x, the breakdown voltage of the AlO_x becomes higher as the temperature of the precursor solution increases when the humidity condition during the spin－coating process is constant. Even, in the case of 40% AlO_x, AlO_x fabricated by the precursor solution of 35 ℃ has 2 times higher breakdown voltage than AlO_x fabricated by the precursor solution of 25 ℃. Meanwhile, when AlO_x is fabricated by the precursor solution of same temperature, the humidity condition during the spin－coating process is divided into two trends. Below 30% humidity, the breakdown voltage decreases as the humidity increases. When humidity is over 40%, AlO_x has a very high breakdown voltage of 5.4 $MVcm^{-1}$ compared to 30% AlO_x whose breakdown voltage is 0.7 $MVcm^{-1}$. And, the breakdown voltage hardly changes when humidity changes. Overall, both precursor solution temperature and humidity condition during the spin－coating process affect the breakdown voltage of AlO_x. More specifically, the effect of the humidity condition during the spin－coating process is greater than that of the precursor solution temperature.

Looking at the change in the leakage current of AlO_x, the tendency of the change in leakage current due to the factors is similar to the

tendency of the change in the breakdown voltage due to the factors. When the humidity condition during the spin−coating process is constant, the leakage current of the AlO_x becomes lower as the temperature of the solution increases. When AlO_x is fabricated by the solution of same temperature, the influence of the humidity condition during the spin−coating process is similarly divided into two trends. Below 30% humidity, the leakage current of AlO_x increases as the humidity increases and this phenomenon is prominent in AlO_x fabricated by the solution at 35 °C. Above 40% humidity, the leakage current becomes very small, $\sim 10^{-6}$ Acm^{-2}, while at 30% humidity the current is $\sim 10^{-1}$ Acm^{-2}.

  Interestingly, the conduction mechanism of leakage current changes from the 40% humidity (**Figure 6**). When the conduction mechanism of leakage current in 30% AlO_x films was compared to that in 40% AlO_x, it can be seen that as the humidity increases, the conduction mechanism of the leakage current significantly changes from the Poole Frankel emission mechanism to the hopping−conduction mechanism.[26] Typically, the change in the current mechanism occurs due to the considerable change in physical or chemical properties in the film.[27] Thus, the chemical or physical properties of AlO_x film changes when fabricated at a humidity condition of 40% or more. To investigate the cause of the changes in electrical characteristics, I analyzed chemical and physical changes according to each factor.

24

Among various models regarding conduction mechanism in insulator film, it is found that the leakage current of 30% AlO_x and 40% AlO_x follow a different model. The conduction mechanism of leakage current in 30% AlO_x follows the Poole−Frankel model. The Poole−Frankel model is as follows:

$$J = q\mu N_c E\, exp\left[\frac{-q(\emptyset_T - \sqrt{(qE/\pi\varepsilon_i\varepsilon_0}}{k_B T}\right]$$

where q is the electronic charge, μ is the electronic drift mobility, N_c is the desity of states in the conduction band, E is the electric field, $q\phi_T$ is the trap energy level, ε_i is the dielectric constant, ε_0 is the permittivity in vacuum. k_B is the Boltzmann constant.

In case of the 40% AlO_x, interestingly, the conduction mechanism of leakage current follows the hopping−conduction model. The hopping−conduction model is as follows:

$$J = qanv\, exp\left[\frac{qaE}{kT} - \frac{E_a}{kT}\right]$$

where a is the mean hopping distance, ν is the thermal vibration frequency of electrons at trap sites, E_a is the activation energy.
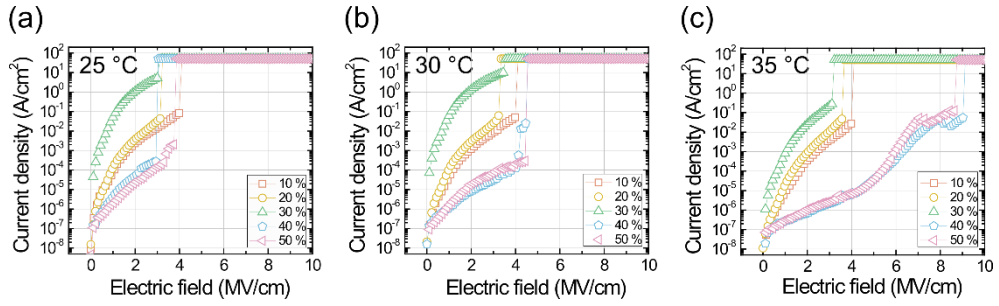
Figure 4. The J−E characteristics of AlO$_x$ films which are fabricated, by precursor solution temperature of (a) 25 ℃, (b) 30 ℃, (c) 35 ℃, and under humidity conditions of 10, 20, 30, 40, 50% during spin-coating process.

	10% AlO$_x$ [MV cm^{-1}]	20% AlO$_x$ [MV cm^{-1}]	30% AlO$_x$ [MV cm^{-1}]	40% AlO$_x$ [MV cm^{-1}]	50% AlO$_x$ [MV cm^{-1}]
25 ℃	1.1	1.0	0.2	2.3	2.8
30 ℃	1.2	1.1	0.2	3.9	3.2
35 ℃	1.7	1.4	0.7	5.4	5.3

Table 1. The breakdown voltage as leakage current density equals 100 μA cm^{-2} of each 10 ~ 50% AlO$_x$ films in 75 samples by one-run.

	10% AlO$_x$ (A cm^{-2})	20% AlO$_x$ (A cm^{-2})	30% AlO$_x$ (A cm^{-2})	40% AlO$_x$ (A cm^{-2})	50% AlO$_x$ (A cm^{-2})
25℃	1.31 x 10^{-2}	2.67 x 10^{-2}	5.22	2.75 x 10^{-4}	1.66 x 10^{-4}
30℃	9.26 x 10^{-3}	2.66 x 10^{-2}	4.60	2.79 x 10^{-5}	6.93 x 10^{-5}
35℃	2.50 x 10^{-3}	8.82 x 10^{-3}	1.37 x 10^{-1}	1.18 x 10^{-6}	2.51 x 10^{-6}

Table 2. The leakage current density at 3 MV cm^{-1} of each 10 ~ 50% AlO$_x$ films in 75 samples by one−run.
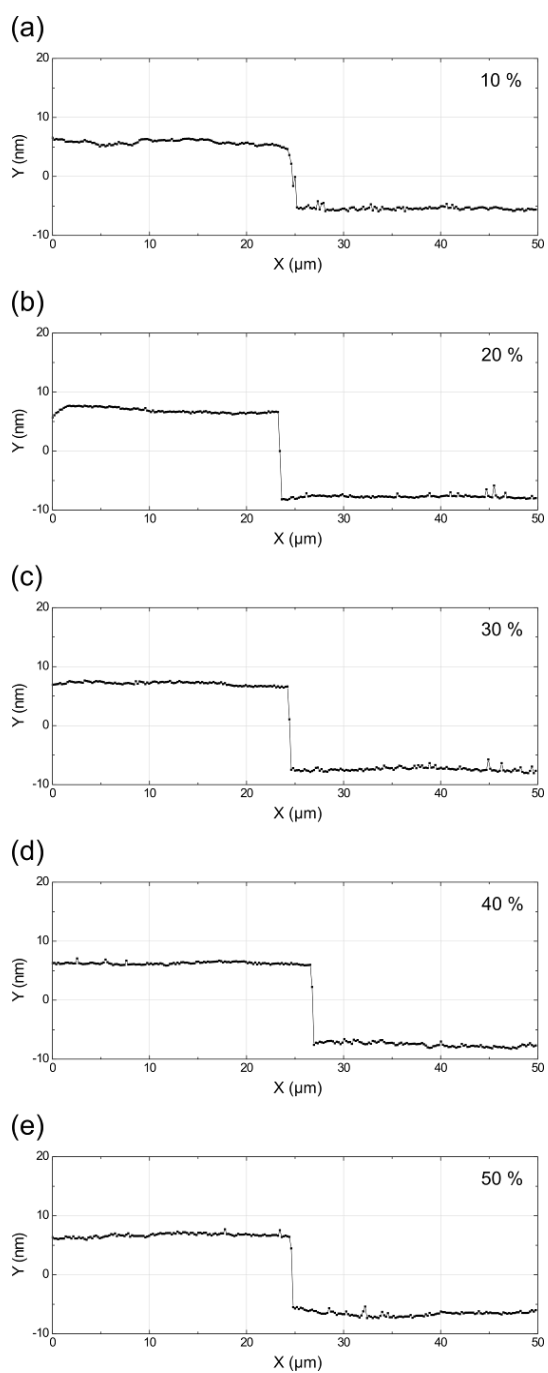
Figure 5. Thickness analyses by AFM on (a) 10%, (b) 20%, (c) 30%, (d) 40%, and (e) 50% AlO$_x$ films.
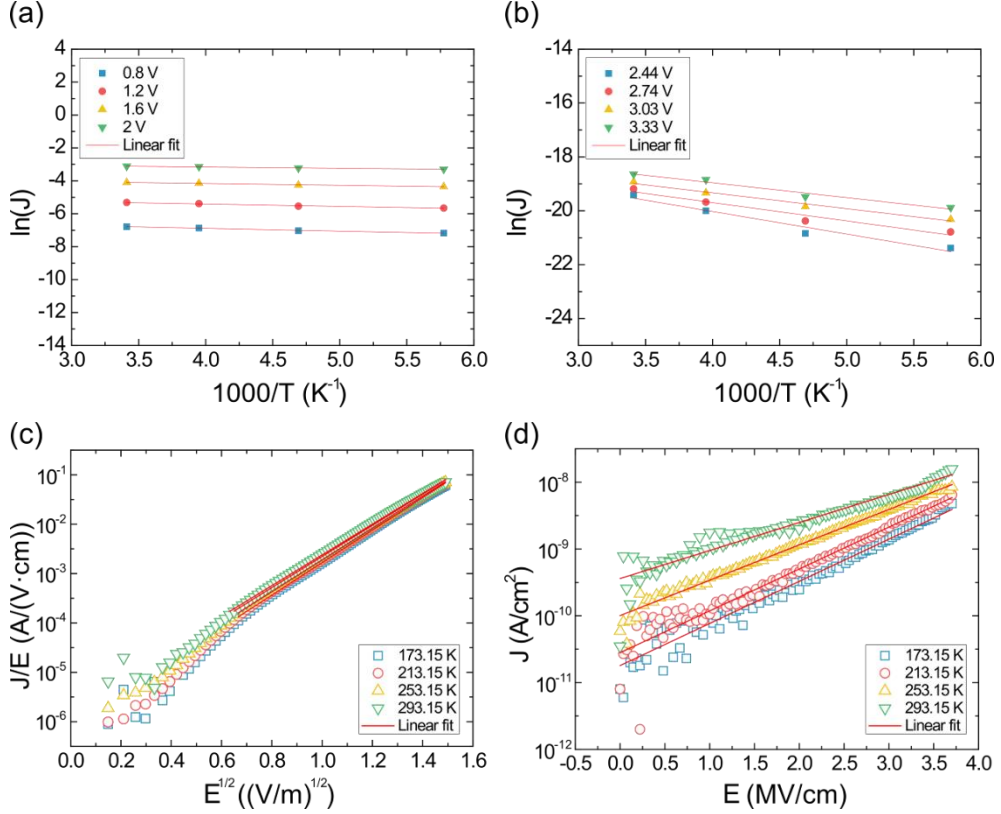
Figure 6. The Arrhenius plot of (a) 30 and (b) 40% AlO$_x$ fabricated by the precursor solution at 35 °C. (c) J/E−E$^{1/2}$ plot of MIM device with 30% AlO$_x$ and (d) J−E plot of MIM device with 40% AlO$_x$.

3.3 Analysis of Effects of Precursor Solution Temperature

Typically, the shapes and behavior of coordination complexes in solution are affected by temperature.[28] When the 25, 30 and 35 ℃ precursor solutions for AlO_x film were analyzed by liquid chromatography－mass spectrometry (LC－MS) (**Figure 7**), they showed a similar tendency. At higher temperature solutions, the peaks at 119.03, 117.07, 208.99, and 331.97 m/z increased while the peak at 256.94 and 314.99 m/z decreased.

 The expected aluminum complexes of the increasing peak are $Al_2O(OH)_3{}^+$ (119.03 m/z), $Al_2(OH)_5(H_2O)_2{}^+$ (117.07 m/z), $Al_2O(OH)_3(H_2O)_5{}^+$ (208.99 m/z), and $Al_{13}O_{18}(OH)_2{}^+$ (331.97 m/z) while the expected aluminum complexes of decreasing peak are $Al_2(OH)_4(NO_3)(H_2O)_4{}^+$ (256.94 m/z), and $Al_3(OH)_7(NO_3)(H_2O)_4{}^+$ (314.99 m/z).[29,30] Overall, at higher temperature solutions, the complexes with nitrate ions decreased while the complexes related to the metal aquo complex is increased (**Figure 8**).

 When the metal aquo complex has higher stability, a higher quality oxide film with fewer defects can be formed.[21] Actually, when AlO_x is analyzed by X－ray Reflectivity (XRR) analysis, the AlO_x film density increased from 2.4629 to 2.6560 gcm^{-3} by rasing the

precursor solution temperature (**Figure 9** and **Table 3**). Typically, a high-quality metal oxide insulator film with fewer defects has less leakage current and higher breakdown voltage.[11] This trend is consistent with the change in density and electrical results of AlO_x thin film depending on the change of precursor solution temperature. Thus, in order to produce higher quality AlO_x thin film with higher breakdown voltage and lower leakage current, a precursor solution with higher temperature leading to more metal aquo complexes is needed.
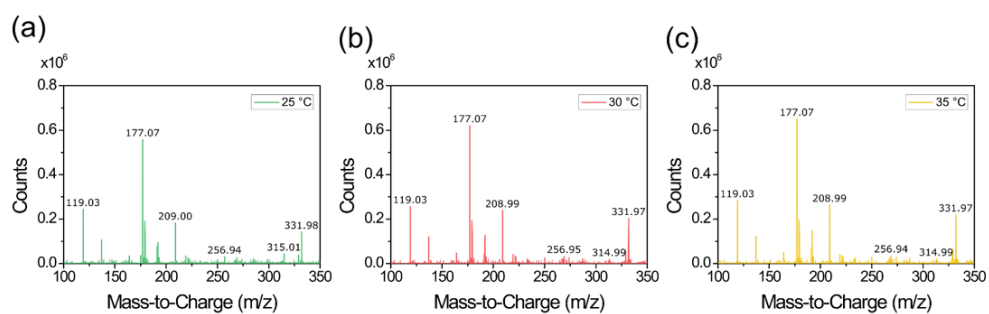
Figure 7. The LC−MS analysis of precursor solutions of which temperature is (a) 25 ℃, (b) 30 ℃, and (c) 35 ℃.
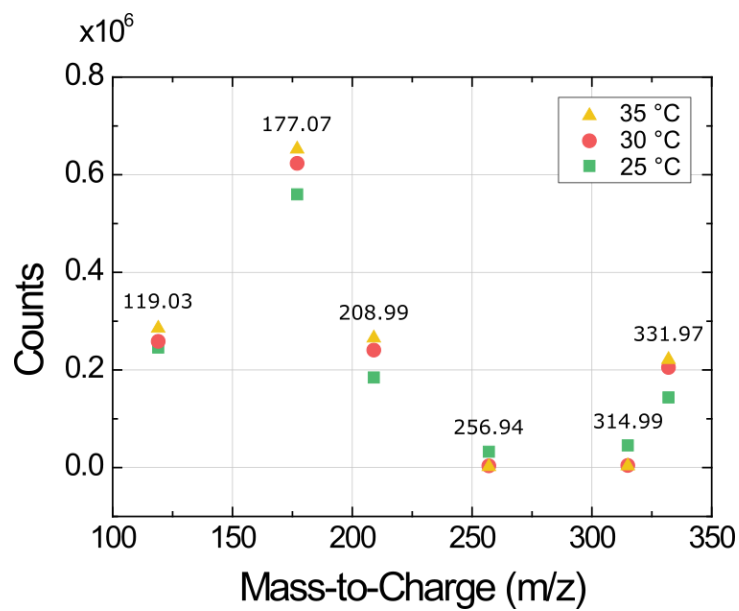
Figure 8. Tendency comparison of LC−MS analysis of 25 ℃, 30 ℃ and 35 ℃ precursor solutions.
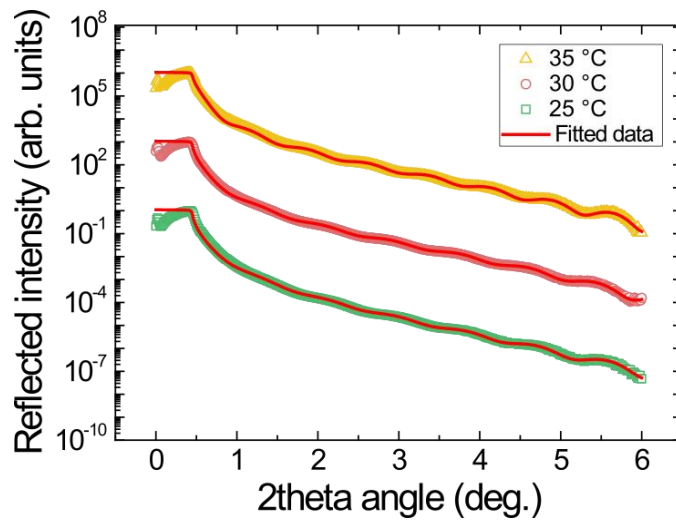
Figure 9. XRR characterization of AlO_x films fabricated by the precursor solutions with 25, 30, and 35 ℃.

	25 ℃ solution	30 ℃ solution	35 ℃ solution
Film density (g/cm^3)	2.4629	2.5499	2.6560

Table 3. The film density of 40% AlO$_x$ fabricated by the diffrent precurosor solution of 25℃, 30℃, and 35℃.

3.4 Analysis of Effects of Humidity Condition during Spin-coating Process

Figure 10 shows the microscope images of the AlO_x thin film surface according to changes in humidity conditions during the spin-coating process. To maintain constant conditions, the temperature of the precursor solution was fixed at 35 ℃, which is the optimized temperature. As shown in Figure 10a-e, as-deposited 10 ~ 30% AlO_x show crack-like surface morphology. Interestingly, the crack-like surface morphology does not appear in the surface for 40 and 50% AlO_x. After the annealing process at 10 ~ 30% AlO_x, the crack seems to have disappeared on the optical microscopy (OM) image. (Figure 10f-j) However, when the surface morphology was examined by the field emission scanning electron microscopy (FESEM), the crack still remained after the annealing process. (**Figure 11**)

When referring to several studies, the crack-like morphology is quite similar to the spherulite structure.[31,32] Typically, it is known that the spherulite structure appears frequently in a minerals and polymers fabricated by the super cooling process.[33,34] In special cases, by rapid evaporation of the solution, the spherulite structure occurs in oxide materials.[33-35] Actually, some researchers have

reported that the spherulite structure can occur at low humidity condition due to rapid evaporation.[35] From this perspective, in the case of aqueous route based AlO_x, a crack-like morphology is the spherulite structure formed under low humidity conditions. Under low humidity conditions (10 ~ 30%), AlO_x films show different spherulite structures depending on humidity, which is very similar to the general spherulite structure forming behavior.[36,37] The surface morphology at 30% AlO_x is the intermediate process of forming the spherulite structure form which is named the hedrite structure.[38] At 20% AlO_x, the surface morphology changes to the branched spherulite structure which is the most common form. At 10% AlO_x, the surface morphology with a smaller and finer-sized spherulite structure is formed.

Several studies show that the spherulite structure acts as a crack in thin films.[39-41] Typically, defects like cracks in films increase leakage current and decrease the breakdown voltage. In fact, 10 ~ 30% AlO_x with spherulite structures show higher leakage currents and lower breakdown voltages than 40 ~ 50% AlO_x. In particular, because the hedrite is intermediate state of spherulite, 30% AlO_x with the hedrite structure gives the low density of internal structure leading to the highest leakage current and lowest breakdown voltage.[42] 40 ~ 50% AlO_x without spherulite structure has a different conduction mechanism for leakage currents than 10 ~ 30% AlO_x. In order for

AlO$_x$ to act as a good insulator, a specific high-humidity condition that does not cause spherulite structures is required.

Figure 10. OM images of as−deposited (a) 10%, (b) 20%, (c) 30%, (d) 40% (e) 50% AlO_x and annealed (f) 10%, (g) 20%, (h) 30%, (i) 40% (j) 50% AlO_x.

As depositioned

(a) 30 %

KANC 15.0kV 8.9mm x5.00k SE(M) 10.0um

(b) 40 %

KANC 15.0kV 9.8mm x5.00k SE(M) 10.0um

After annealing

(c) 30 %

KANC 15.0kV 8.8mm x5.00k SE(M) 10.0um

(d) 40 %

KANC 15.0kV 9.3mm x5.00k SE(M) 10.0um
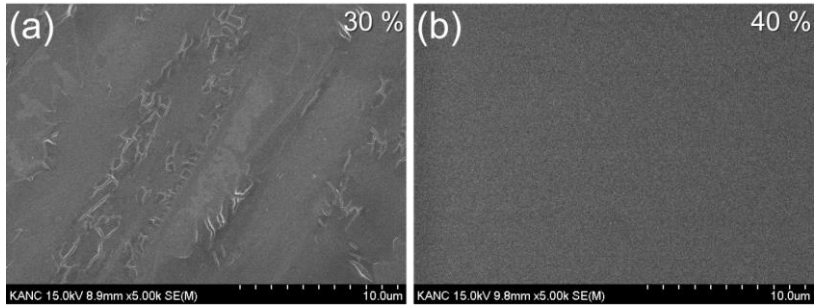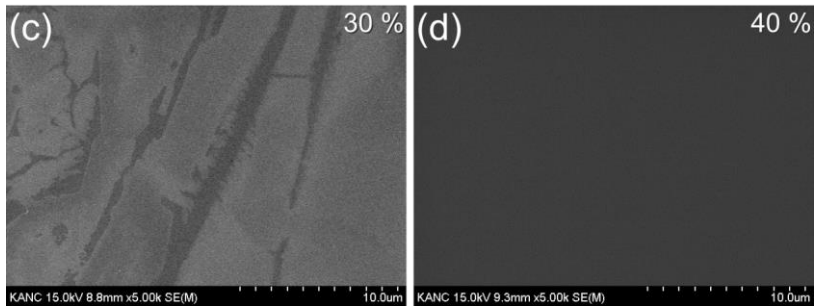
Figure 11. FESEM images of as-deposited (i) 30%, (j) 40% AlO_x and annealed (i) 30%, (j) 40% AlO_x.

3.5 Electrical Performance of InO$_x$ TFT Based on Optimized AlO$_x$ Insulator

In order to verify that AlO$_x$ fabricated at optimized conditions would have the same optimum conditions when applied to electrical devices, an evaluation of the electrical characteristics through TFT application has been carried out. **Figure 12** and **Table 4** show electrical properties of InOx TFTs with 10 ~ 50% AlO$_x$. In this process, all devices are patterned by the photolithography process (**Figure 13**). In addition, the temperature of the precursor solution was fixed at 35 ℃ for AlO$_x$ film fabrication, because AlO$_x$ fabricated by solutions at different temperatures has too high of a leakage current and does not show normal characteristics when applied to TFT. All the transfer characteristics were measured by a gate−source voltage (V$_{gs}$) from −1 to 4.5 V and a drain−source voltage (V$_{ds}$) at 1 V. Typically, the leakage current in the linear region decreases the drain current, so that the drain current behavior of the TFTs varies depending on the magnitude of the leakage current (**Figure 14**). Looking at the InO$_x$ TFT with 10 ~ 30% AlO$_x$ that has detailed transfer characteristics (**Figure 15**), the off−current is high and drain current drops below a certain gate voltage due to the high leakage current is high. When the transfer characteristics are viewed on a linear scale, the decrease in

the drain current due to the leakage current can be seen clearly compared with that in transfer characteristics viewed on a log scale (**Figure 16**). Otherwise, InO_x TFTs with 40 and 50% AlO_x have a low off-current and operate as normal with low leakage current (**Figure 17, Figure 18**, and Figure 15). Furthermore, InO_x TFTs with 40 and 50% AlO_x exhibit critical levels of average field-effect mobilities of 52.33 $cm^2V^{-1}s^{-1}$ and 15.27 $cm^2V^{-1}s^{-1}$, respectively. (The field-effect mobility was calculated by the areal capacitance (~560 $nFcm^{-2}$, $\kappa = \sim 9$) measured at low frequency conditions (0.5 Hz) (**Figure `19** and **Table 5**)). Meanwhile, InO_x TFTs with 40% AlO_x show little anticlockwise-like hysteresis of 0.4 V (**Figure 20**), which are considered impure ions that hardly disappear completely in solution-processed dielectrics.[43] Considering the hysteresis is very small and the change of the capacitance value according to the change of the frequency is not large (Figure 19 and Table 5), it is expected that the amount is considerably small.

Capacitance measurements were performed to investigate the AlO_x insulator property depending on humidity during spin-coating with $p^{++}Si/AlO_x/Al$ capacitor. Capacitance was measured by two instruments. One measures the low-frequency range from 0.5 Hz to 200 Hz and the other measures the range from 20 Hz to 1 MHz. Capacitance measurements of 30% AlO_x at low frequency are not shown because the capacitance value cannot be measured due to

extremely high leakage current. The capacitances of 10, 20, 40, and 50% AlO_x are 520.58±6.12, 562.01±5.88, 561.12±6.10, and 555.14±5.8, relatively. It can be confirmed that 10% and 20% AlO_x have lower capacitance due to high leakage current.

Overall, it was confirmed that AlO_x fabricated during the optimum conditions exhibited good performance when applied to a TFT. Interestingly, although 40 and 50% AlO_x have similar electrical properties, InO_x TFTs with 40 and 50% AlO_x exhibit different field−effect mobility characteristics and the surface roughness is similar (**Figure 21**). When the leakage current of the TFT is checked, the leakage current of InO_x with 50% AlO_x is considerably larger than that of InO_x 40% AlO_x. Therefore, InO_x with 50% AlO_x has small mobility due to the decrease of drain current compared to InO_x with 40% AlO_x. This makes it possible to deduce that the electrical performance of 50% AlO_x as an insulator changes when InO_x is deposited by a solution process on AlO_x. This suggests that further investigation is needed on the critical factors when oxide films fabricated by the solution process are chemically interacted.
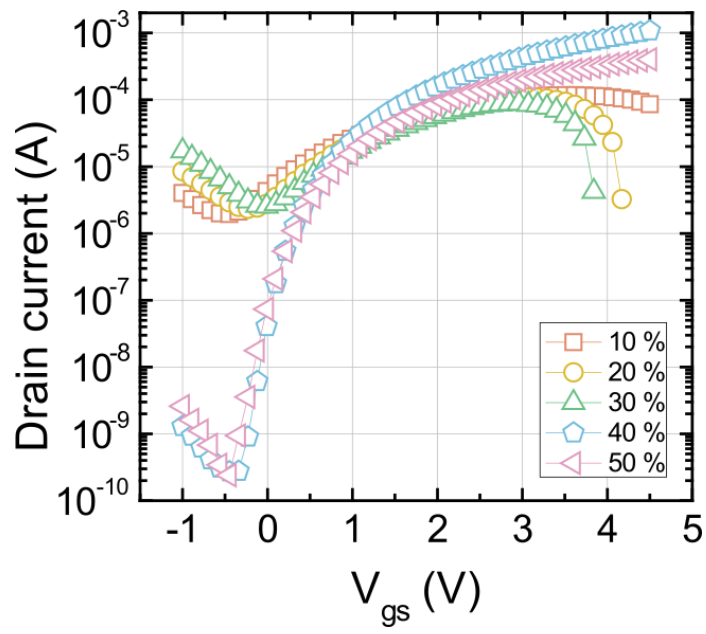
Figure 12. Transfer characteristics of InO_x TFTs with 10, 20, 30, 40, and 50% AlO_x.

	10% AlO$_x$	20% AlO$_x$	30% AlO$_x$	40% AlO$_x$	50% AlO$_x$
Field−effect mobility (cm^2/Vs)	−	−	−	52.33 ±3.22	15.27 ±2.20
On/off current ratio	6 x 10^2	6 x 10^2	3 x 10^2	4 x 10^6	2 x 10^6

Table 4. Field−effect mobility and on/off current ratio of patterned InO$_x$ TFTs with 10 ~ 50% AlO$_x$ in 50 samples by one−run. The ″−″ means the region where field−effect mobility cannot be obtained.
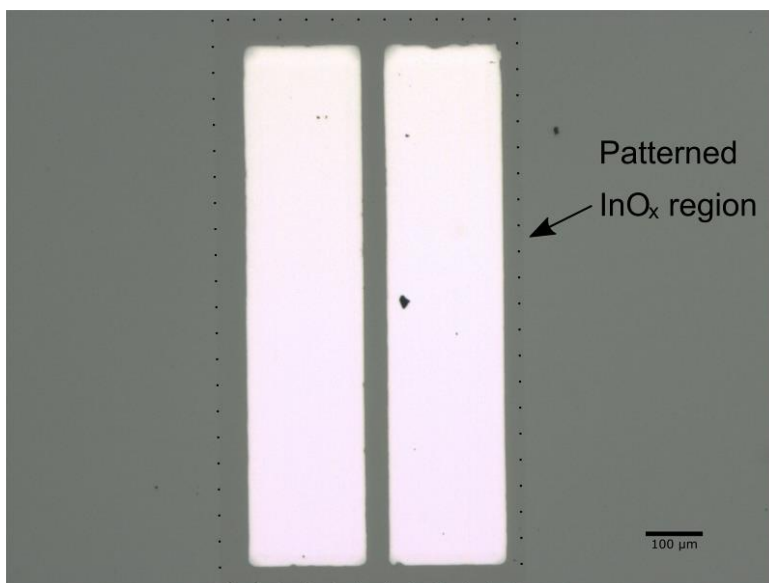
Figure 13. OM image of patterned InO_x TFT with AlO_x.
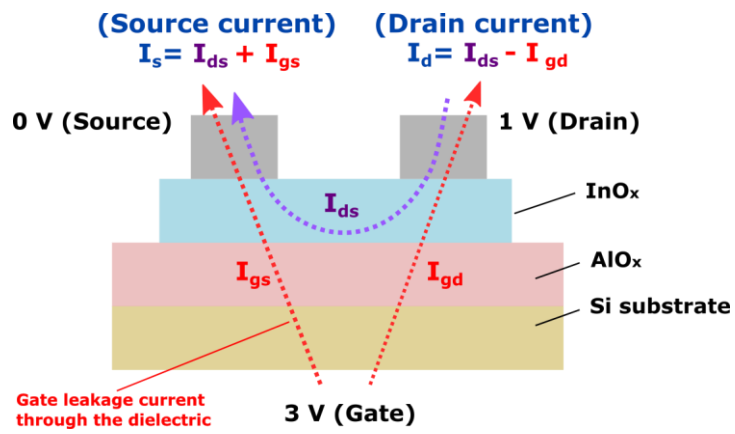
Figure 14. The schematic of current flows in the InO_x TFT with AlO_x.
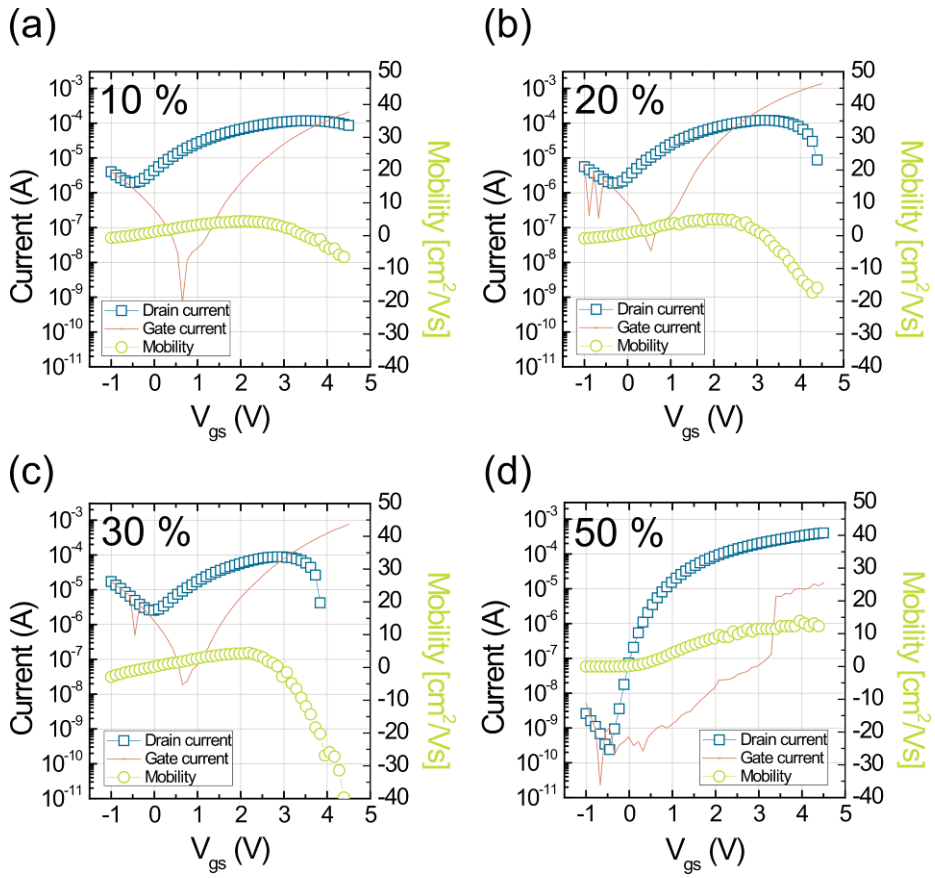
Figure 15. Transfer characteristics of InOx TFTs with (a) 10%, (b) 20%, (c) 30%, and (d) 50% AlOx.
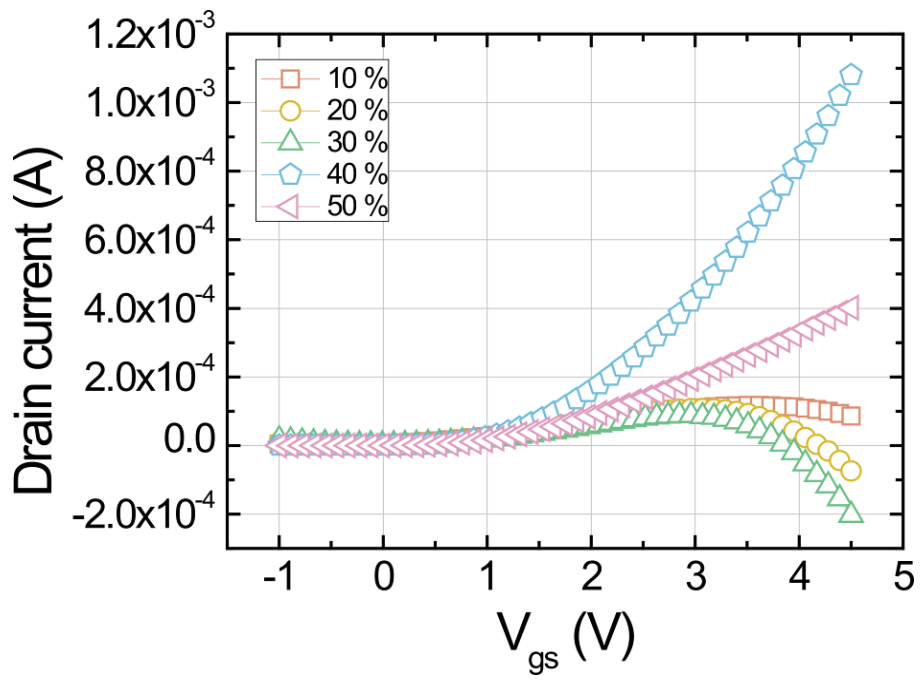
Figure 16. Transfer characteristics set y−axis as linear scale of InO_x TFTs with 10 ~ 50% AlO_x.
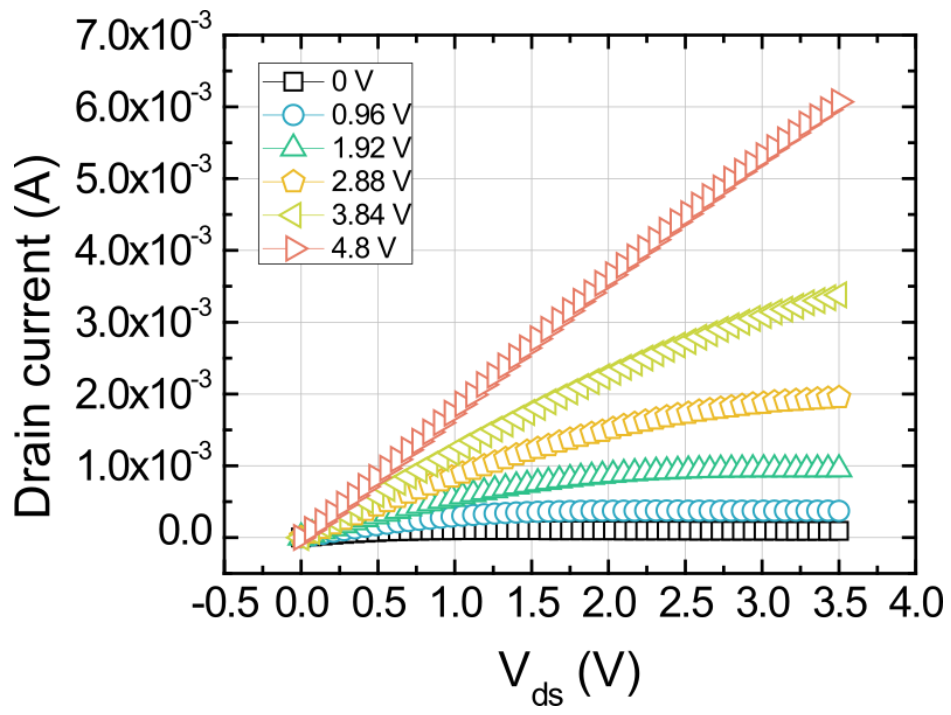
Figure 17. Output characteristics of InO_x TFT with 40% AlO_x.
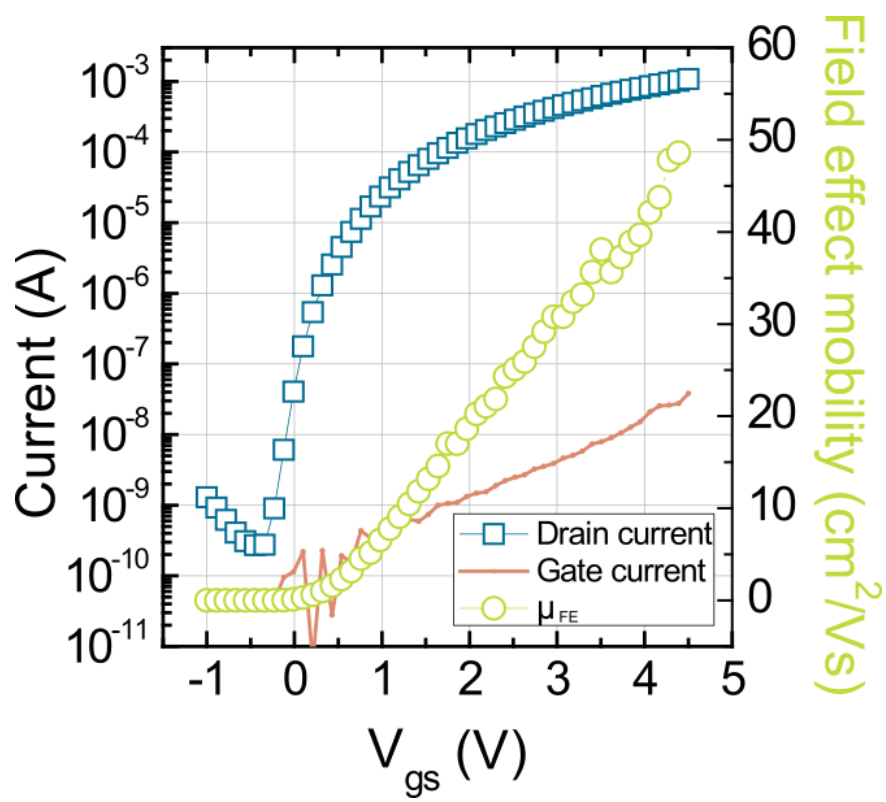
Figure 18. Detailed transfer characteristics of InO_x TFT with 40% AlO_x.
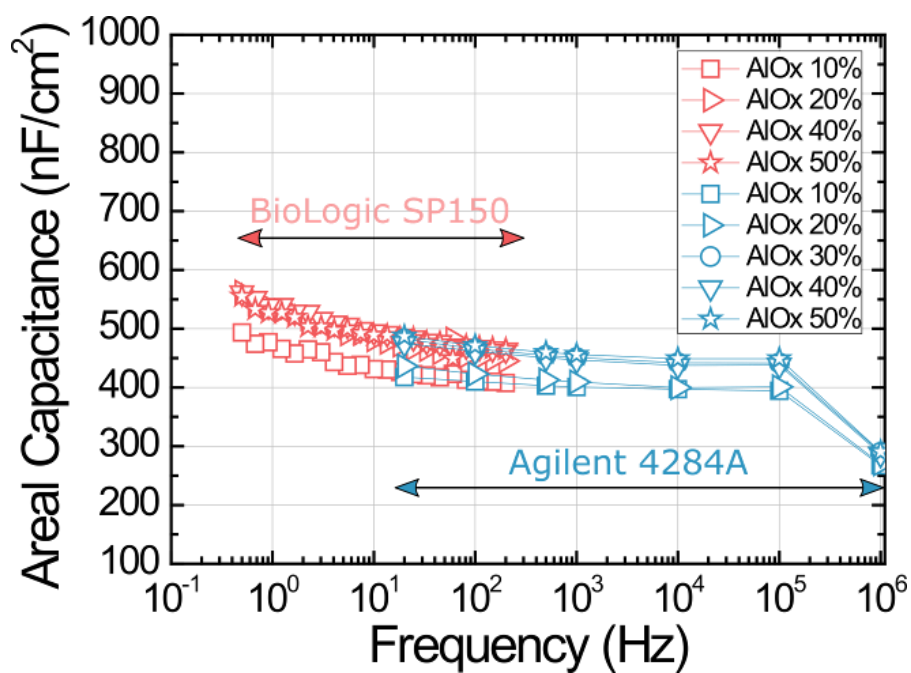
Figure 19. Capacitance values of 10, 20, 30, 40, and 50% AlO$_x$ measured from, 0.5 Hz to 200 Hz by BioLogic SP150, and 20 Hz to 1 kHz by Agilent 4284A.

	10% AlO$_x$	20% AlO$_x$	30% AlO$_x$	40% AlO$_x$	50% AlO$_x$
Capacitance (nF/cm^2)	520.58 ±6.12	562.01 ±5.88	–	561.12 ±6.10	555.14 ±5.80

Table 5. Areal capacitance of 10 ~ 50% AlO$_x$ measured at 0.5 Hz condition in 25 samples by one-run.
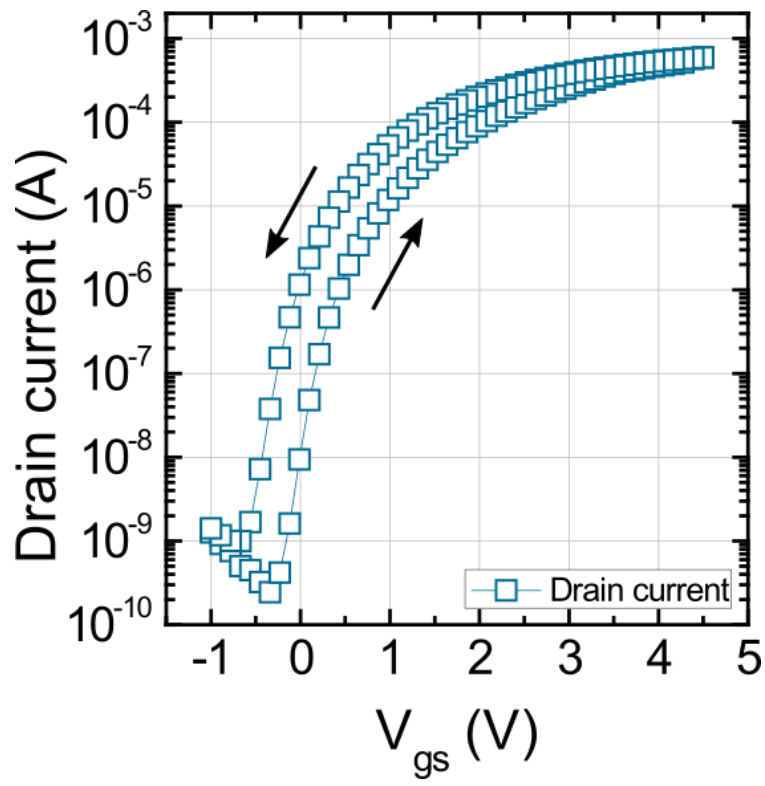
Figure 20. Hysteresis characteristics of InO_x TFT with 40% AlO_x.

(a)

40 %

(b)

50 %
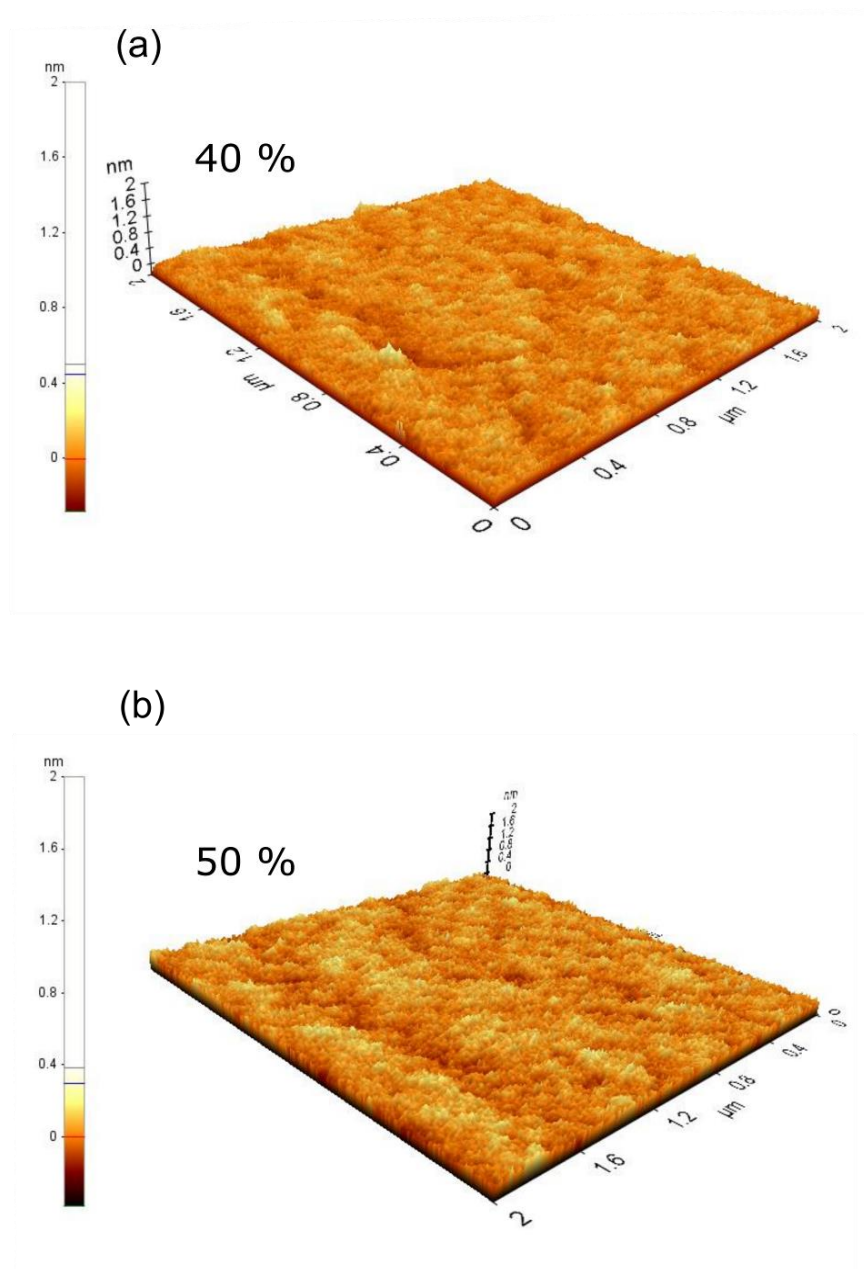
Figure 21. AFM images of the (a) 40% and (b) 50% AlO$_x$ films.

Chapter 4. Conclusion

 In summary, controlling the precursor solution temperature and the humidity conditions during the spin－coating process are important for developing high－quaility metal oxide insulators and AlO_x thin films based on the aqueous route method. Through the electrical evaluation of AlO_x fabricated by a precursor solution of specific temperature (25, 30, and 35 ℃), and under specific humidity conditions during the spin－coating process (10, 20, 30, 40, and 50%), it was confirmed that breakdown voltage and leakage current of AlO_x are considerably changed depending on critical factors. By various AFM, LC－MS, XRR, OM, and SEM analyses, it was confirmed that the changes in electrical properties are related to changes in chemical and physical properties in AlO_x films. Furthermore, the mechanism of the changes in chemical and physical film properties according to critical factors was found. In essence, the higher the precursor solution temperature, more complexes related to the metal aquo complex were formed, which increased the film density and electrical performance. In terms of humidity conditions during the spin－coating process when AlO_x is fabricated under conditions of 30% humidity or less, the surface morphology of the spherulite structure, which can act as a crack, can be formed. Accordingly, AlO_x fabricated under conditions of 30% humidity shows higher leakage currents and lower

breakdown voltages. The conduction mechanism of leakage current changes at the 40% humidity condition. Finally, optimized AlO_x film based on the aqueous route method is fabricated when the precursor solution temperature is 35 °C and the humidity during the spin-coating process is 40%. In order to verify that AlO_x fabricated at optimized conditions would act at the same optimum conditions in the electrical devices, the AlO_x was applied to the InO_x TFT. Finally, by introducing optimized conditions which is the precursor solution temperature of 35 °C and 40% humidity condition during the spin-coating process, I successfully achieved InO_x/AlO_x TFTs showing high average field-effect mobility of ~ 52 $cm^2V^{-1}s^{-1}$ and on/off current ratio of 10^6 at annealing temperature of 250 °C. I believe that this study regarding critical factors for high-quality metal oxide insulator thin film development based on the aqueous route method provides a good basis for low-temperature and solution-processed metal oxide insulator development for a wide range of electrical applications.

.

References

1.   Kamiya, T.; Nomura, K.; Hosono, H., Present status of amorphous In-Ga-Zn-O thin-film transistors. *Science and Technology of Advanced Materials* **2010**, 11, 1-23.

2.   Fortunato, E.; Barquinha, P.; Martins, R., Oxide Semiconductor Thin-Film Transistors: A Review of Recent Advances. *Advanced Materials* **2012**, 24, 2945-2986.

3.   Kim, S.; Choi, Y. J.; Choi, Y.; Kang, M. S.; Cho, J. H., Large-Area Schottky Barrier Transistors Based on Vertically Stacked Graphene-Metal Oxide Heterostructures. *Advanced Functional Materials* **2017**, 27, 1700651.

4.   Yu, X. G.; Marks, T. J.; Facchetti, A., Metal oxides for optoelectronic applications. *Nature Materials* **2016**, 15, 383-396.

5.   Pal, B. N.; Dhar, B. M.; See, K. C.; Katz, H. E., Solution-deposited sodium beta-alumina gate dielectrics for low-voltage and transparent field-effect transistors. *Nature Materials* **2009**, 8, 898-903.

6.   Kim, Y. H.; Heo, J. S.; Kim, T. H.; Park, S.; Yoon, M. H.; Kim, J.; Oh, M. S.; Yi, G. R.; Noh, Y. Y.; Park, S. K., Flexible metal-oxide devices made by room-temperature photochemical activation of sol-gel films. *Nature* **2012**, 489, 128-U191.

7.   Kim, M. G.; Kanatzidis, M. G.; Facchetti, A.; Marks, T. J., Low-temperature fabrication of high-performance metal oxide thin-film

electronics via combustion processing. *Nature Materials* **2011**, 10, 382-388.

8.   Park, S. Y.; Kim, B. J.; Kim, K.; Kang, M. S.; Lim, K. H.; Il Lee, T.; Myoung, J. M.; Baik, H. K.; Cho, J. H.; Kim, Y. S., Low-Temperature, Solution-Processed and Alkali Metal Doped ZnO for High-Performance Thin-Film Transistors. *Advanced Materials* **2012**, 24, 834-+.

9.   Park, J. H.; Kim, K.; Yoo, Y. B.; Park, S. Y.; Lim, K. H.; Lee, K. H.; Baik, H. K.; Kim, Y. S., Water adsorption effects of nitrate ion coordinated Al_2O_3 dielectric for high performance metal-oxide thin-film transistor. *Journal of Materials Chemistry C* **2013**, 1, 7166-7174.

10.   Kim, J.; Lim, S. H.; Kim, Y. S., Solution-Based TiO2-Polymer Composite Dielectric for Low Operating Voltage OTFTs. *Journal of the American Chemical Society* **2010**, 132, 14721-14723.

11.   Park, S.; Kim, C. H.; Lee, W. J.; Sung, S.; Yoon, M. H., Sol-gel metal oxide dielectrics for all-solution-processed electronics. *Materials Science & Engineering R-Reports* **2017**, 114, 1-22.

12.   Banger, K. K.; Yamashita, Y.; Mori, K.; Peterson, R. L.; Leedham, T.; Rickard, J.; Sirringhaus, H., Low-temperature, high-performance solution-processed metal oxide thin-film transistors formed by a 'sol-gel on chip' process. *Nature Materials* **2011**, 10, 45-50.

13.   Meyers, S. T.; Anderson, J. T.; Hung, C. M.; Thompson, J.; Wager, J. F.; Keszler, D. A., Aqueous Inorganic Inks for Low-Temperature Fabrication of ZnO TFTs. *Journal of the American Chemical Society* **2008**, 130, 17603-17609.

14.   Hwang, Y. H.; Seo, J.-S.; Yun, J. Moon; Park, H.; Yang, S.; Ko Park, S.-H.; Bae, B.-S. An 'aqueous route' for the fabrication of low-temperature-processable oxide flexible transparent thin-film transistors on plastic substrates. *NPG Asia Mater.* **2013**, 5, e45.

15.   Lim, K. H.; Huh, J. E.; Lee, J.; Cho, N. K.; Park, J. W.; Nam, B. I.; Lee, E.; Kim, Y. S., Strong Influence of Humidity on Low-Temperature Thin-Film Fabrication via Metal Aqua Complex for High Performance Oxide Semiconductor Thin-Film Transistors. *ACS Appl Mater Interfaces* **2017**, 9, 548-557.

16.   Plassmeyer, P. N.; Mitchson, G.; Woods, K. N.; Johnson, D. C.; Page, C. J., Impact of Relative Humidity during Spin-Deposition of Metal Oxide Thin Films from Aqueous Solution Precursors. *Chemistry of Materials* **2017**, 29, 2921-2926.

17.   Lee, K. H.; Park, J. H.; Yoo, Y. B.; Han, S. W.; Lee, S. J.; Baik, H. K., Modulation of aqueous precursor solution temperature for the fabrication of high-performance metal oxide thin-film transistors. *Applied Physics Express* **2015**, 8, 081101.

18.   Lee, K. H.; Han, S. W.; Park, J. H.; Yoo, Y. B.; Lee, S. J.; Baik, H. K.; Song, K. M., Low temperature fabrication of metal oxide thin film transistors formed by a heated aqueous precursor solution. *Japanese Journal of Applied Physics* **2016**, 55, 010304.

19.   Seo, J. S.; Jeon, J. H.; Hwang, Y. H.; Park, H.; Ryu, M.; Park, S. H. K.; Bae, B. S., Solution-Processed Flexible Fluorine-doped Indium Zinc Oxide Thin-Film Transistors Fabricated on Plastic Film at Low Temperature. *Scientific Reports* **2013**, 3.

20.   Faber, H.; Lin, Y. H.; Thomas, S. R.; Zhao, K.; Pliatsikas, N.;

McLachlan, M. A.; Amassian, A.; Patsalas, P. A.; Anthopoulos, T. D., Indium Oxide Thin-Film Transistors Processed at Low Temperature via Ultrasonic Spray Pyrolysis. *ACS Applied Materials & Interfaces* **2015**, 7, 782-790.

21.   Rim, Y. S.; Chen, H.; Song, T.-B.; Bae, S.-H.; Yang, Y., Hexaaqua Metal Complexes for Low-Temperature Formation of Fully Metal Oxide Thin-Film Transistors. *Chemistry of Materials* **2015**, 27, 5808-5812.

22.   Liu, A.; Liu, G.; Zhu, H.; Shin, B.; Fortunato, E.; Martins, R.; Shan, F., Eco-friendly water-induced aluminum oxide dielectrics and their application in a hybrid metal oxide/polymer TFT. *RSC Adv.* **2015**, 5, 86606-86613.

23.   Xu, W.; Cao, H.; Liang, L.; Xu, J. B., Aqueous Solution-Deposited Gallium Oxide Dielectric for Low-Temperature, Low-Operating-Voltage Indium Oxide Thin-Film Transistors: A Facile Route to Green Oxide Electronics. *ACS Appl Mater Interfaces* **2015**, 7, 14720-5.

24.   Liu, G.; Liu, A.; Zhu, H.; Shin, B.; Fortunato, E.; Martins, R.; Wang, Y.; Shan, F., Low-Temperature, Nontoxic Water-Induced Metal-Oxide Thin Films and Their Application in Thin-Film Transistors. *Advanced Functional Materials* **2015**, 25, 2564-2572.

25.   Liu, A.; Liu, G. X.; Zhu, H. H.; Song, H. J.; Shin, B.; Fortunato, E.; Martins, R.; Shan, F. K., Water-Induced Scandium Oxide Dielectric for Low-Operating Voltage n- and p-Type Metal-Oxide Thin-Film Transistors. *Advanced Functional Materials* **2015**, 25, 7180-7188.

26.   Chiu, F.-C., A Review on Conduction Mechanisms in Dielectric Films.

Advances in Materials Science and Engineering **2014**, 2014, 1−18.

27.   Hasegawa, A.; Tanno, T.; Nogami, S.; Satou, M., Property change mechanism in tungsten under neutron irradiation in various reactors. *Journal of Nuclear Materials* **2011**, 417, 491−494.

28.   Alberty, R. A., Standard Gibbs Free Energy, Enthalpy, and Entropy Changes as a Function of Ph and Pmg for Several Reactions Involving Adenosine Phosphates. *Journal of Biological Chemistry* **1969**, 244, 3290−&.

29.   Urabe, T.; Tsugoshi, T.; Tanaka, M., Characterization of aluminum species with nitrate, perchlorate and sulfate ions in the positive and negative ion mode by electrospray ionization mass spectrometry. *J Mass Spectrom* **2009**, 44, 193−202.

30.   Sarpola, A.; Hietapelto, V.; Jalonen, J.; Jokela, J.; Laitinen, R. S.; Rämö, J., Identification and fragmentation of hydrolyzed aluminum species by electrospray ionization tandem mass spectrometry. *Journal of Mass Spectrometry* **2004**, 39, 1209−1218.

31.   Bräuer, B.; Zahn, D. R. T.; Rüffer, T.; Salvan, G., Deposition of thin films of a transition metal complex by spin coating. *Chemical Physics Letters* **2006**, 432, 226−229.

32.   Haque, N.; Cochrane, R. F.; Mullis, A. M., Morphology of Spherulites in Rapidly Solidified Ni3Ge Droplets. *Crystals* 2017, 7.

33.   Keith, H. D.; Padden, F. J., A Phenomenological Theory of Spherulitic Crystallization. *Journal of Applied Physics* **1963**, 34, 2409−&.

34.   Shtukenberg, A. G.; Punin, Y. O.; Gunn, E.; Kahr, B., Spherulites. *Chem Rev* **2012**, 112, 1805−38

35.   Gunn, E., Small molecule banded sphemlites. Ph.D. Dissertation,

University of Washington, Seattle, Washington, USA **2009**.

36.   Hegde, R. R.; Spruiell, J. E.; Bhat, G. S., Investigation of the morphology of polypropylene - nanoclay nanocomposites. *Polymer International* 2014, 63, 1112-1121.

37.   Wang, Y.; Liu, X. F.; Peng, J.; Qiu, F., Controlling morphology and crystalline structure in poly(3-hexylselenophene) solutions during aging. *Rsc Advances* **2015**, 5, 107970-107976

38.   Beekmans, L. G. M.; Vancso, G. J., Real-time crystallization study of poly(epsilon-caprolactone) by hot-stage atomic force microscopy. *Polymer* **2000**, 41, 8975-8981.

39.   Niazi, M. R.; Li, R.; Qiang Li, E.; Kirmani, A. R.; Abdelsamie, M.; Wang, Q.; Pan, W.; Payne, M. M.; Anthony, J. E.; Smilgies, D. M.; Thoroddsen, S. T.; Giannelis, E. P.; Amassian, A., Solution-printed organic semiconductor blends exhibiting transport properties on par with single crystals. *Nat. Commun.* **2015**, 6, 8598.

40.   Woo, E.; Lugito, G., Cracks in Polymer Spherulites: Phenomenological Mechanisms in Correlation with Ring Bands. *Polymers* **2016**, 8, 329.

41.   Zhang, C.; Lu, L.; Li, W.; Li, L.; Zhou, C., Effects of crystallization temperature and spherulite size on cracking behavior of semi-crystalline polymers. *Polymer Bulletin* **2016**, 73, 2961-2972.

42.   Viswanath, V.; Maity, S.; Bochinski, J. R.; Clarke, L. I.; Gorga, R. E., Thermal Annealing of Polymer Nanocomposites via Photothermal Heating: Effects on Crystallinity and Spherulite Morphology. *Macromolecules* **2013**, 46, 8596-8607.

43.   Egginger, M.; Bauer, S.; Schwödiauer, R.; Neugebauer, H.; Sariciftci,

N. S., Current versus gate voltage hysteresis in organic field effect transistors. *Monatshefte für Chemie – Chemical Monthly* **2009**, 140, 735–750.

요약(국문초록)

최근에, 금속 아쿠아 착물을 이용한 물 용매를 사용한 방법은 저온 제조 조건에서 높은 전기 특성을 갖는 용액 처리 된 금속 산화물 박막을 제조할 수 있기 때문에 많은 주목을 받고 있다. 그러나, 대부분의 연구는 주로 금속 산화물 반도체 박막의 개발에 집중되었다. 수성 경로 기반의 금속 산화물 필름을 다양한 플렉서블 소자에 광범위하게 적용하기 위해서는 수성 경로 방법을 통해 만들어진 금속 산화물 절연체 필름에 대한 체계적인 연구가 요구된다.

본 연구에서는 수성 경로 방법을 기반으로 한 고 품질, 고 성능 금속 산화물 절연체 박막을 개발하기 위한 결정적인 요소 두 가지를 제안하였다. 실험을 통해 전구체 용액 온도와 스핀 코팅 공정 동안의 습도가 AlOx 절연체 박막 제작 시 박막의 화학적, 물리적 및 전기적 특성에 큰 영향을 미치는 것으로 나타났습니다. 이러한 결정적인 요인을 최적화하여 최적화되지 않은 AlOx보다 누설 전류 값이 약 105배 작고 약 2 ~ 3 배 큰 항복 전압 값을 갖는 AlOx 절연체 박막을 구현하였다. 최종적으로 최적화 된 AlOx 절연체 박막을 용액공정을 통해 만들어진 InOx를 반도체 박막으로 사용한 TFT에 도입함으로써 250 ℃의 저온 공정에서도 ~ 52 cm2V-1s-1의 높은 이동도, 106의 온/오프 전류비를 가진 InOx/AlOx TFT를 성공적으로 구현하였다

....

주요어 : 수성경로, 유전체, 산화 알루미늄, 금속 아쿠아 착이온, 박막 트랜지스터

학 번 : 2016-26028